Title	Development of a ZnS/$^{10}B_2O_3$ scintillator with low-afterglow phosphor
Author(s)	Nakamura Tatsuya, Katagiri Masaki, Tsutsui Noriaki, To Kentaro, Rhodes N. J., Schooneveld E. M., Oguri Hirofumi, Noguchi Yasunobu, Sakasai Kaoru, Soyama Kazuhiko
Citation	Journal of Physics; Conference Series, 528, p.012043_1-012043_8
Text Version	Published Journal Article
URL	https://jopss.jaea.go.jp/search/servlet/search?5041477
DOI	https://doi.org/10.1088/1742-6596/528/1/012043
Right	Content from this work may be used under the terms of the Creative Commons Attribution 3.0 licence. Any further distribution of this work must maintain attribution to the author(s) and the title of the work, journal citation and DOI. Published under licence by IOP Publishing Ltd

Development of a ZnS/$^{10}B_2O_3$ scintillator with low-afterglow phosphor

2014 J. Phys.: Conf. Ser. 528 012043

(http://iopscience.iop.org/1742-6596/528/1/012043)

Development of a ZnS/$^{10}B_2O_3$ scintillator with low-afterglow phosphor

T Nakamura[1], M Katagiri[2], N Tsutsui[3], K Toh[1], N J Rhodes[4], E M Schooneveld[4], H Ooguri[5], Y Noguchi[5], K Sakasai[1] and K Soyama[1]

[1] J-PARC center, Japan Atomic Energy Agency, Tokai, Ibaraki 319-1195, Japan
[2] Frontier Research Center for Applied Atomic Sciences, Ibaraki University, Tokai, Ibaraki 319-1106, Japan
[3] Chichibu Fuji Co. Ltd, Chichibu, Saitama 368-0193, Japan
[4] ISIS, Rutherford Appleton Laboratory, Chilton, Oxfordshire OX11 0QX, UK
[5] NICHIA, Anan, Tokushima 774-8601, Japan

E-mail:nakamura.tatsuya@jaea.go.jp

Abstract. A low-afterglow, ^{10}B-doped neutron-sensitive ZnS/$^{10}B_2O_3$ scintillator was developed. The developed ZnS phosphor has a primary decay time constant of about 60 ns with a low afterglow. The developed scintillator exhibited a mean afterglow height of 4% relative to the peak at 1 μs after the peak, which is half that of a commercial ZnS/^{6}LiF scintillator manufactured by Applied Scintillation Technologies. The count-rate capability of a wavelength-shifting-fibre-based detector was increased to 30,000 cps by implementing the developed scintillator from 5,000 cps with the commercial scintillator.

1. Introduction

^{6}Li-doped ZnS scintillators have been used extensively in thermal-neutron detection in many neutron-scattering instruments at various pulsed-neutron facilities, including at the ISIS in the UK and the SNS in the USA [1, 2]. The properties of these scintillators of a high light yield with an excellent capability to discriminate neutrons and gamma rays make them potentially suitable for constructing large-area position-sensitive detectors for use in neutron-scattering experiments. Also, ZnS/^{6}LiF scintillators can easily be constructed in sheet form, making them economically efficient. This is particularly important for neutron-scattering instruments that require many detector modules to cover a large scattering angle around a sample.

One of the challenges in using a ZnS scintillator is improving its count-rate capability. The commercial ZnS:Ag phosphor is known to have a high light yield of ~160,000 photons in the nuclear reaction ^{6}Li(n,α)T, but it also exhibits a high afterglow that lasts for more than 100 μs [3, 4]. The pulse pileup associated with this afterglow hinders neutron detection at a high count rate, and becomes particularly problematic for a detector used at a MW-class pulsed-neutron source, such as in the Materials and Life Science Experimental Facility at the Japan Proton Accelerator Research Complex (J-PARC/MLF).

There are several neutron-sensitive scintillator materials that exhibit a faster time response than the ZnS:Ag/^{6}LiF scintillator. A Ce-activated ^{6}Li glass scintillator is known to have a typical decay time of 50–70 ns [5]. However, the gamma-ray sensitivity of a ^{6}Li glass scintillator is one to two orders of

magnitude higher than that of a ZnS/^{6}LiF scintillator. Other types of Ce-doped scintillator have been developed with moderate gamma-ray sensitivities, while the capability for gamma-ray rejection can be increased using pulse-shape discrimination, such as with $Li_6Gd(BO_3)_3$ [6], Cs_2LiYCl_6 [7] or $LiCaAlF_6$ [8]. However, the light yields of such materials are more than an order of magnitude lower than for ZnS, which makes them unsuitable for constructing a large-area position-sensitive detector that is coupled to optical fibres in neutron-scattering instruments.

This paper presents a new neutron-sensitive ZnS:Ag-based scintillator that achieves a high light yield, low afterglow contamination and low gamma-ray sensitivity with a reasonable manufacturing cost. The count-rate capability of a wavelength shifting fibre (WLS)-based detector implemented with a ZnS/$^{10}B_2O_3$ scintillator was also evaluated.

2. Neutron-sensitive ZnS:Ag scintillator with low afterglow

2.1. Sample preparation

Table 1 summarizes the details of the samples used in experimental evaluations. Two types of neutron-sensitive ZnS scintillator screens were prepared for the evaluations using the low-afterglow ZnS phosphor: ZnS:Ag/$^{10}B_2O_3$ and ZnS:Ag /^{6}LiF. The fabrication methods are summarized below; further details are available elsewhere [9].

A ZnS:Ag powder with a low afterglow and a particle size of about 5 μm was prepared in-house [10] and mixed with $H_3{}^{10}BO_3$ at a mass ratio of 1.0~1.5. The composite powder was poured onto a 0.3-mm-thick aluminium base plate that was placed in an electronic furnace and sintered for 3 hours at 540 °C. $H_3{}^{10}BO_3$ becomes glassy when it melts, water escapes and it becomes $^{10}B_2O_3$. The $^{10}B_2O_3$ melts at 480°C and it acts as a binder material. The resultant material is ZnS/$^{10}B_2O_3$ ceramic scintillator. The nominal ^{10}B enrichment rate exceeded 90%.

A polycrystalline ^{6}LiF powder with a mean particle diameter of about 10 μm was used as a converter material when constructing the ZnS/^{6}LiF scintillator. An inorganic binder was added to the ZnS powder, and the mixed composite was poured onto an aluminium base plate to form a scintillator sheet. The nominal ^{6}Li enrichment factor was 90%.

Table 1. Properties of the scintillator samples.

Scintillator type	Sample number	ZnS type (manufacturer)	ZnS: $H_3{}^{10}BO_3$ or ^{6}LiF (by weight)	Coating amount (mg/cm^2) $H_3{}^{10}BO_3$ or ^{6}LiF	Total	N*t value [b] (x10^{20}, 1/cm^2)
ZnS/$^{10}B_2O_3$	No 1	tst13-no3 (JAEA)	1.00 : 1	30.0	60.0	2.5
	No 2	tst13-no1 (JAEA)	1.14 : 1	26.3	56.0	2.1
	No 3	tst14-no1 (JAEA)	1.33 : 1	22.5	52.0	1.8
	No 4	tst13-no2 (JAEA)	1.50 : 1	20.0	50.0	1.6
	No 5	tst14-no3 (JAEA)	1.15 : 1	32.5	70.0	2.7
	No 6	1109-041 (NICHIA)	1.25 : 1	30.0	67.0	2.5
	No 7	amt6-no3 (JAEA)	1.36 : 1	27.5	65.0	2.3
	No 8	amt6-no3 (JAEA)	1.50 : 1	25.0	62.5	2.1
ZnS/^{6}LiF	No 1	amt6-no3 (JAEA)	1.00 : 1	30.0	60.0	5.9
	No 2	amt6-no3 (JAEA)	1.20 : 1	30.0	66.0	5.9
	No 3	amt6-no3 (JAEA)	1.50 : 1	30.0	75.0	5.9
References [a]	AST(2:1)	--	2.00 : 1	~24	~72	~4.7
	AST(4:1)	--	4.00 : 1	~15	~80	~2.8

a) ZnS/^{6}LiF from AST. Coating amounts were determined from the experimental results.
b) N*t values is the product of the density of the neutron-conveter material and the thickness of the samples.

The commercial product, a ZnS/^{6}LiF-based scintillator manufactured by Applied Scintillation Technologies (AST), was also prepared as a reference. This ZnS/^{6}LiF neutron screen is constructed from polycrystalline ZnS mixed with a ^{6}LiF converter material, which provides thermoplastic characteristics.

2.2. Experimental setup

A bialkali photomultiplier tube (PMT; Model 9102B, ET Enterprises) was used to record neutron-induced signals. An iris mask constructed from a 15-μm-thick aluminium foil was attached to the PMT to give a neutron-sensitive area of 10 × 10 mm^2. A test sample was attached directly to the PMT through the iris mask using optical grease. The scintillator sample and PMT detector were irradiated with neutrons from an Am-Be source with a radioactivity of 3.7×10^{11} Bq. The neutrons from the Am-Be source were thermally moderated with a polyethylene moderator that had a volume of 1200 × 1200 × 1200 mm^3. Neutron-induced signals were recorded with a 12-bit digitizer (Model U1065A, Acqiris), and the signal waveforms were analyzed. The count rate on the detector was typically below 100 cps, and hence the count loss of the measurement system was negligible.

3. Results and discussion

3.1. Signal waveform

Figure 1 shows averaged neutron-induced signal waveforms of the samples (signal waveforms of the typical three samples were shown in the figure). These samples exhibited similar primary emission decays. An exponential fit of the primary decay indicated a 1/ε time constant of ~60 ns. The afterglow was much lower for both the developed ZnS/$^{10}B_2O_3$ and ZnS/^{6}LiF scintillators than for the reference AST scintillator, which demonstrates that the prepared low-afterglow ZnS:Ag phosphor was effective at reducing the afterglow.

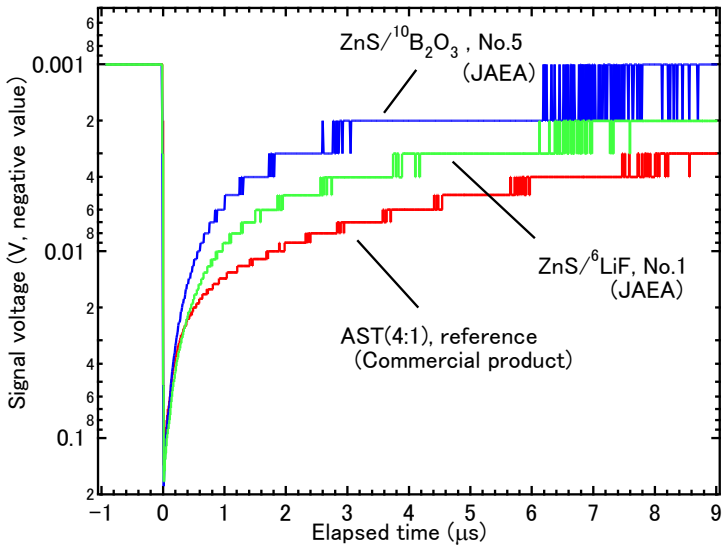

Figure 1. Averaged waveforms of neutron-induced signals measured by the bialkali PMT (Model 9102B, ET Enterprises). The signals shown are means of 9400 waveforms.

Figure 2a, b and c show the (a) signal pulse height at the peak, (b) signal pulse height at 1μs after the peak time and (c) the ratio of the signal heights at 1 μs after the peak time and at a peak time (called the "afterglow rate" hereafter). The peak height was similar among all of the samples, including the reference AST(2:1) scintillator (Figure 2a), at 0.14–0.20 V. On the other hand, the pulse height at 1 μs after the peak time was significantly lower for the developed samples (Figure 2b): the

afterglows of the ZnS/$^{10}B_2O_3$ and ZnS/^{6}LiF scintillators were about 40% and 60% of the reference value, respectively. This decrease in the afterglow was clearly evident in the pulse shapes normalized by their own peak heights, with afterglow rates of 2.7–4.0%, 5.5–5.7% and 9.0–10.1% for the ZnS/$^{10}B_2O_3$, ZnS/^{6}LiF and reference AST scintillators, respectively (Figure 2c). The afterglow rates varied slightly with the converter materials and mixing ratios of the composite materials; these effects should be clarified in future studies.

The neutron absorption probability, ε, is described as follows,

$$\varepsilon = 1 - e^{-N \cdot t \cdot \sigma}$$

where, N is a density of neutron-converter material, t is a thickness of the scintillator, and σ is a neutron-absorption cross-section. The neutron absorption probabilities of each sample were calculated by using the product of N and t shown in the Table 1.

Figure 3 shows that the measured neutron count rate as a function of the calculated neutron absorption probability. The measured count rate was higher for samples with the larger N and t

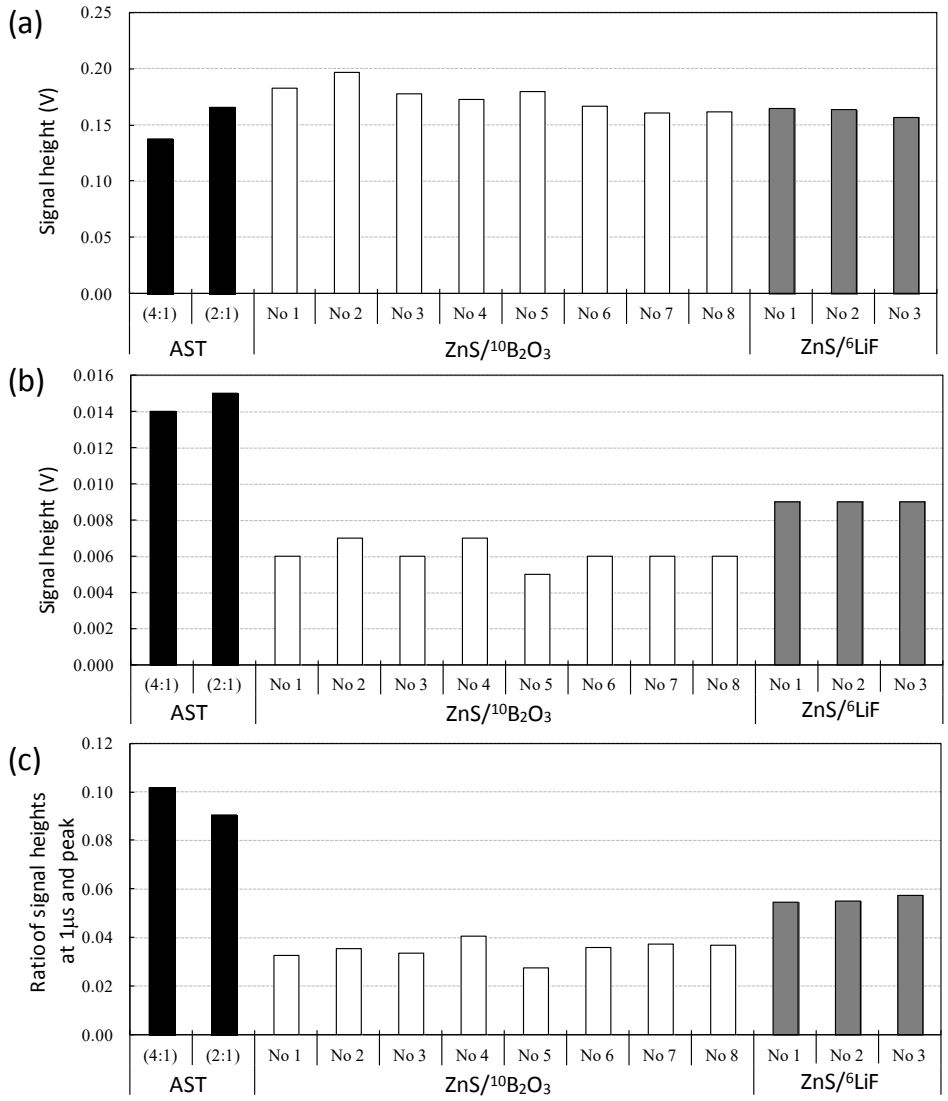

Figure 2. Signal heights (a) at the peak and (b) at 1 μs after a peak. (c) Ratio of signal heights in (a) and (b).

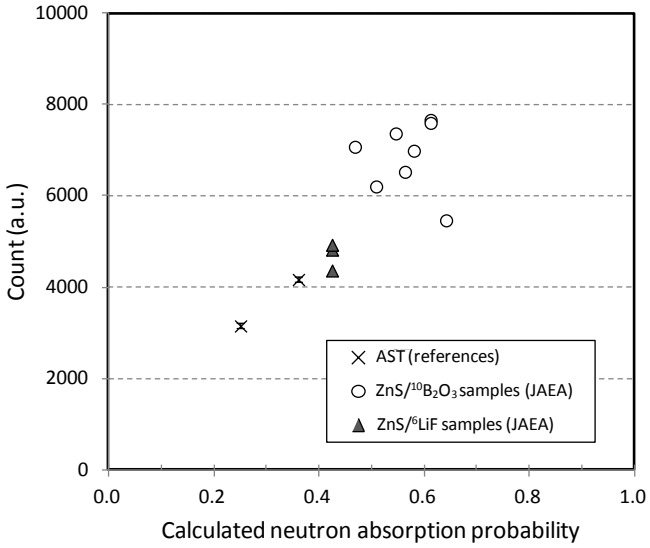

Figure 3. Scatter plot of the measured neutron count versus the calculated neutron absorption probability for the samples.

product. Moreover, the neutron count was higher for the ^{10}B-doped ZnS scintillator than for scintillators doped with ^{6}LiF. This result indicated that using the ZnS/$^{10}B_2O_3$ allowed the construction of a detector with a high detection efficiency in our particular samples.

In general the detection efficiency of a ZnS scintillator is strongly affected by the neutron absorption rate and the light transmittance of a sample since ZnS is opaque to its own emission light. Predicting the light transmittance is also of particular difficult since it is contributed by many factors such as scintillator thickness, grain size, light attenuation length, particle track length. In practice precise measurements of light transmission were also difficult due to the use of an aluminium base plate in our samples. The experimental finding of a highly linear correlation between the neutron absorption rate and measured counts indicated that the prepared samples had similar light

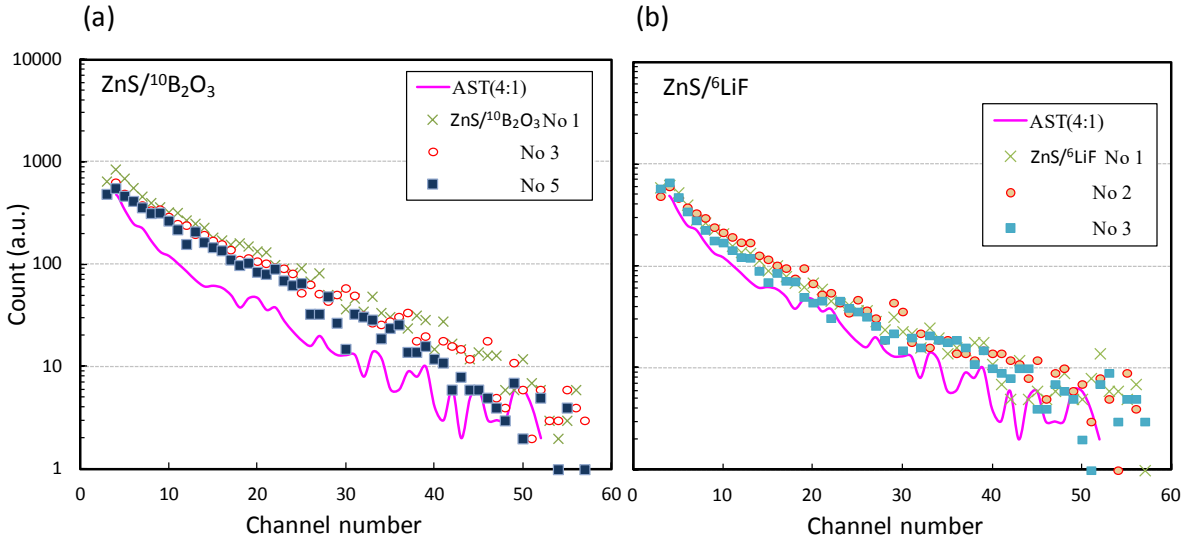

Figure 4. Pulse height distribution of (a) ZnS/$^{10}B_2O_3$ and (b) ZnS/^{6}LiF constructed using the ZnS scintillator with a low afterglow. Pulse height distribution of the AST(4:1) scintillator is included as reference.

transmittances. Figure 4 shows measured pulse height distributions of typical samples measured while irradiating with neutrons. All of the other samples also had similar neutron-induced signal heights, which supports the above interpretation.

Figure 5 is a scatter plot of the measured neutron count versus the afterglow rate, which represent the detection efficiency and count-rate capability of the implemented detector, respectively. The data for our samples were clearly separated each other, with the ZnS/$^{10}B_2O_3$ scintillator exhibiting the highest neutron count rate and the lowest afterglow rate, thereby ensuring a detector with a high detection efficiency and good count-rate capability.

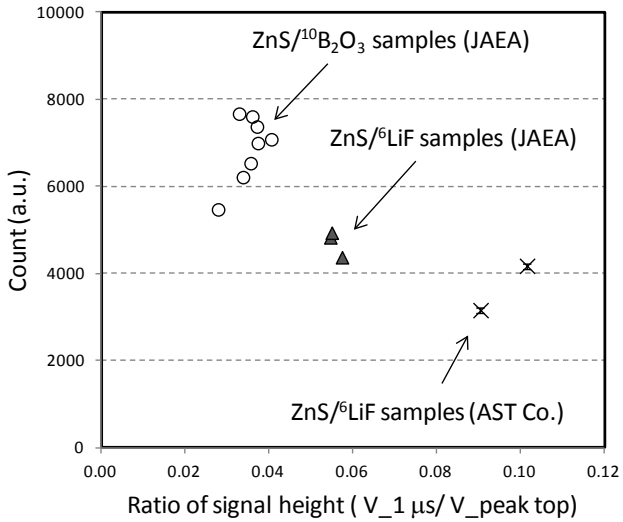

Figure 5. Scatter plot of the measured neutron count versus the afterglow rate, defined as the ratio of the signal height at 1 μs after the peak time to that at the peak time.

3.2. Detector performance with the ZnS/$^{10}B_2O_3$ ceramic scintillator

The count-rate capability of the ZnS/$^{10}B_2O_3$ scintillator was evaluated using a WLS-fibre-based

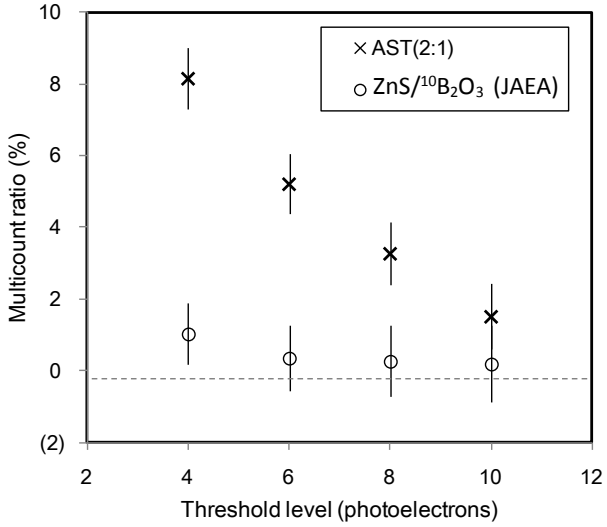

Figure 6. Multicount ratio of the ZnS/$^{10}B_2O_3$ (JAEA, No1) and the AST(2:1) scintillators measured by the scintillator/WLS-fibre detector that was developed for the SENJU instrument at J-PARC/MLF.

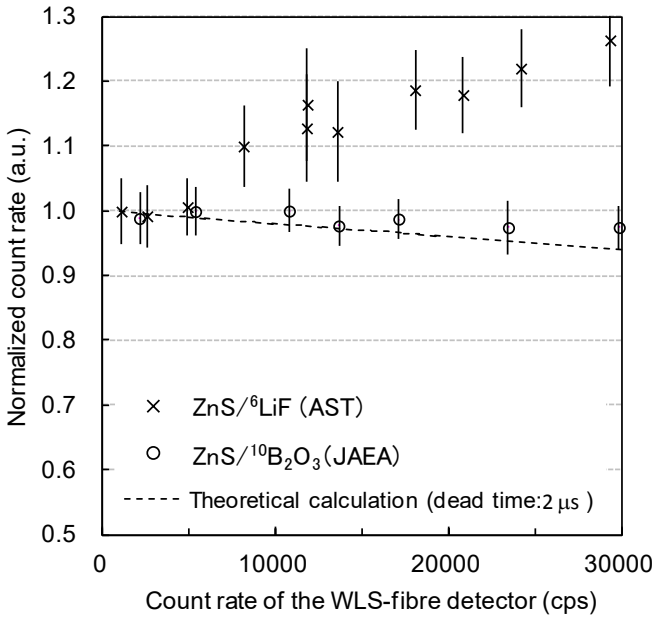

Figure 7. Normalized count rate of the WLS-fibre detectors implemented with the reference scintillator and the ZnS/$^{10}B_2O_3$ scintillator screen, respectively.

detector. The detector comprised 64 × 2 WLS fibre arrays, with the WLS fibres placed at a regular pitch of 4 mm in both the *x* and *y* directions [11]. The ZnS/$^{10}B_2O_3$ scintillator screen constructed from the composite indicated as No. 1 in Table 1 was used for this test. Two scintillator screens sandwiched the WLS fibre arrays in the detector.

Prior to the test at a reactor, the multicount rate of the detector was evaluated using a ^{252}Cf neutron source. The multicount rate is defined as the probability of counting single neutrons more than once, and such an event can result from the afterglow of the scintillation light, making it a good indicator of the count-rate capability of a detector. To evaluate the effect of the afterglow to the count rate no specific signal processing method was implemented to system such as inserting a dead time.

Figure 6 shows the multicount rates for the detectors implemented with the ZnS/$^{10}B_2O_3$ and AST(2:1) scintillators as functions of the threshold level. The counts produced by trigger pulses with widths of 100 ns and 20 μs were compared; the latter counts were considered the true counts without multicount contamination. The multicount rate was in the range of 2–8% for the reference AST scintillator when measured with a threshold level of 4–10 photoelectrons, and was about an order of magnitude lower for the developed ZnS/$^{10}B_2O_3$ scintillator, at 0.1–0.5%. Multicount events occur mainly due to a high afterglow during ZnS scintillation, and hence the developed low-afterglow ZnS/$^{10}B_2O_3$ scintillator was quite effective.

The count-rate capability of the detector was evaluated using a cold-neutron beam at the CHOP port in Japanese Research Reactor 3 at Japan Atomic Energy Agency. The cold-neutron beam had a peak wavelength of 4Å and was collimated into a size of 5 × 5 mm^2, with the beam illuminating the centre region of the neutron-sensitive area. Figure 7 shows the normalized count rates of the detectors implemented with the reference scintillator and the ZnS/$^{10}B_2O_3$ scintillator screen. The count rate of the detector was divided by the count measured by a detector monitoring the incident neutrons (a ^{3}He detector with a detection efficiency of ~10^{-4} for thermal neutrons), with the resultant normalized ratio facilitating comparisons with the theoretical calculations. Since this monitored count is proportional to the true incident rate (i.e. with negligible count loss), the count ratio should be

$$n_{wlsf} / n_{monitor} \propto 1 - n_{wlsf} \cdot \tau_{wlsf}$$

where n_{wlsf} and $n_{monitor}$ are the count rates measured by the WLS-fibre detector and the monitoring detector, respectively, and τ_{wlsf} is the dead time of the WLS detector (which was ~2 μs in the test detector system). The count ratio for the reference AST scintillator deviated from the calculated value when the incident rate exceeded 5,000 cps, which was due to the presence of significant afterglow. This deviation increased approximately proportionally with the incident count rate, reaching about 30% for a count rate of 30,000 cps. In contrast, the count rate of the developed ZnS/$^{10}B_2O_3$ scintillator followed the calculated value up to 30,000 cps within experimental errors. This clear decrease in multicount events can be attributed to the lower afterglow of the developed scintillator.

4. Summary

We have developed a ZnS/$^{10}B_2O_3$ ceramic scintillator constructed using a ZnS phosphor that has a low afterglow for neutron-scattering instruments at J-PARC/MLF. The ZnS/$^{10}B_2O_3$ ceramic scintillator exhibited the best performance of the prepared samples, exhibiting both a high detection efficiency and a low multicount rate. The count-rate capability of the ZnS/$^{10}B_2O_3$ ceramic scintillator was evaluated in combination with a WLS-based detector, which demonstrated that the developed scintillator was effective at minimizing the multicount event rate and also improving the count-rate capability of the detector.

References

[1] ISIS facility: http://www.isis.stfc.ac.uk/
Regarding the detectors installed in the ISIS, for example, Rhodes N J, Schooneveld E M and Eccleston R S 2004 *Nucl. Instr.& Meth*. A **529** 243
[2] SNS facility: http://neutrons.ornl.gov/
[3] Rhodes N J 1996 *Proc. of SCINT95 (Delft)* (Delft: Delft University Press) p 73
[4] van Eijk C W E 2001 *Nucl. Instr. & Meth*. A **460** 1
[5] Fairley E J and Spowart A R 1978 *Nucl. Instr. & Meth.* **150** 159
[6] Czir J B, MacGillivray G M, MacGillivray R R and Seddon P J 1999 *Nucl. Instr. & Meth.* A **424** 15
[7] Bessiere A, Dorenbos P, van Eijk C W E, Krämer and Güdel H U 2005 *Nucl. Instr. & Meth.* A **537** 242
[8] Getkin A, Shiran N, Neicheva S, Gavrilyuk, Bensalah A, Fukuda T and Shimamura K 2002*Nucl. Instr. & Meth.* A **486** 274
[9] Kojima T, Katagiri M, Tsutsui N, Imai K, Matsubayashi M and Sakasai K 2004 *Nucl. Instr. & Meth.* A **529** 325
[10] Katagiri M. in private communication
[11] Nakamura T, et al 2012 *Nucl. Instr. & Meth.* A **686** 64.